Klein-Gordon versus relativistic Schrödinger equations in pion-nucleus scattering

R. J. McLeod
School of Physical Sciences, The Flinders University of South Australia, Bedford Park, SA, 5042, Australia
(Received 10 December 1993)

The relativistic Schrödinger equation and the Klein-Gordon equation for an optical potential for pion scattering are investigated in the resonance energy region and at higher energies. Previous calculations showed that the two equations give nearly the same results with the difference decreasing with increasing energy. We find a substantial difference between the two approaches for π^+ on ^{40}Ca at 180 MeV. This difference persists even at 500 MeV. The difference is partly due to the different off-shell behaviors and partly due to the different propagators used. At small angles in the resonance region, the difference can be understood as an energy shift at which the two-body t matrix is evaluated or as a different range of the two-body interaction.

PACS number(s): 24.10.Jv, 25.80.Dj, 24.10.Ht

Relativistic pion-nucleus scattering has been calculated by using an optical potential in both the Klein-Gordon equation (KGE) [1] and the relativistic Schrödinger equation (RSE) [2]. Previously, the results of using these two different approaches have been nearly the same when using a factorized approximation to the optical potential for pion energies in the resonance region [3,4]. We show that when the Fermi integral is performed the two approaches give a different result, not only in the resonance region, but for energies as high as 500 MeV. At 180 MeV, the different off-shell behaviors and the different propagators used give rise to the observed differences found in the differential cross sections. At small angles at resonance energies, this difference can be understood as a shift in the energy at which one evaluates the π-Nt matrix or as a change in the effective range of the π-N interaction in the P_{33} channel. At 500 MeV, the different off-shell behavior is primarily responsible for the observed difference.

We examine the scattering of π^+ on ^{40}Ca at 180, 292.5, and 500 MeV. These calculations are made by using a first order optical potential that is generated by performing the Fermi integral. This is the main difference to earlier calculations. This optical potential is then used in solving the RSE and the KGE. The impulse approximations is used for consistency with previous results.

To see the connection between the KGE and the RSE we follow Johnson and Ernst [3]. In their notation, the KGE for an optical potential can be written as

$$\psi_{\rm KG}(\mathbf{k};\mathbf{t}) = \phi(\mathbf{k};\mathbf{t}) + \int \frac{d^3t'}{(2\pi)^3} \frac{\langle \mathbf{t}|U_{\rm KG}|\mathbf{t}'\rangle}{k^2 - t^2 + i\eta} \psi_{\rm KG}(\mathbf{k};\mathbf{t}'), \tag{1}$$

where the Green's function operates between the optical potential U and the wave function ψ. The propagator can be decomposed by rewriting it as

$$\frac{1}{k^2 - t^2 + i\eta} = \frac{1}{2\omega_t} \frac{1}{\omega_k - \omega_t + i\eta} - \frac{1}{2\omega_t} \frac{1}{\omega_k + \omega_t}. \tag{2}$$

By dropping the second term and making the substitutions

$$\psi_{\rm KG}(\mathbf{k};\mathbf{t}) = \left(\frac{\omega_k}{\omega_t}\right)^{1/2} \psi_{\rm RS}(\mathbf{k};\mathbf{t}) \tag{3}$$

and

$$\langle \mathbf{t}|U_{\rm RS}|\mathbf{t}'\rangle = (2\omega_t)^{-1/2} \langle \mathbf{t}|U_{\rm KG}|\mathbf{t}'\rangle (2\omega_t')^{-1/2} \tag{4}$$

into Eq. (1) we find

$$\psi_{\rm RS}(\mathbf{k};\mathbf{t}) = \phi(\mathbf{k};\mathbf{t}) + \int \frac{d^3t'}{(2\pi)^3} \frac{\langle \mathbf{t}|U_{\rm RS}|\mathbf{t}'\rangle}{\omega_k - \omega_t + i\eta} \psi_{\rm RS}(\mathbf{k};\mathbf{t}'). \tag{5}$$

This is the RSE for an optical potential.

We can see that the two equations are the same except for the second term in Eq. (2). The RSE has only intermediate pions that propagate forward in time while the KGE has in addition pions propagating backward in time. The second term in Eq. (2) gives rise to these pions and thus to crossing in the KGE. In the static limit, this crossing symmetry is maintained in the KGE if it is in the two-body input [5].

The second element that is changed between the two equations is the off-shell behavior. For the KGE we use a Chew-Low behavior which is consistent with the field theoretic nature of the KGE. For the RSE we use the separable potential behavior which is consistent with the potential approach used in the RSE. These are the preferred options for the respective equations [6,7] being the consistent off-shell behavior for the propagators used. The separable potential form factors are given by

$$v_{\rm SP}(k) = \omega^{1/2}(k) k^l e^{-k^2/\beta^2}. \tag{6}$$

The Chew-Low vertex functions are related to the separable potential form factors by [6,11]

$$v_{\rm CL}(k) = \omega^{1/2}(k) v_{\rm SP}(k). \tag{7}$$

The optical potential is written as [8]

$$\langle \mathbf{P}'_1\mathbf{P}'_A|U(E)|\mathbf{P}_1\mathbf{P}_A\rangle = \sum_{\alpha_3}\int \frac{d^3P_3}{2\bar{E}_3}\langle\Psi'(\mathbf{P}'_A)|\mathbf{P}_2\mathbf{P}_3\alpha_3\rangle\langle\mathbf{P}'_1\mathbf{P}'_2|t(E)|\mathbf{P}_1\mathbf{P}_2\alpha_3\rangle \times\langle\mathbf{P}_2\mathbf{P}_3\alpha_3|\Psi(\mathbf{P}_A)\rangle. \quad (8)$$

Equation (8) is written in a three-body formalism where particles 1, 2, and 3, are the pion, the nucleon in the A-nucleon target, and the residual $A-1$ nucleon core, respectfully. $t(E)$ is the two-body pion-nucleon t matrix and Ψ and Ψ' are the nucleon wave function before and after the nucleon interacts with the pion. The nucleons in the nucleus are summed over and α_3 denotes a set of quantum numbers that label the nucleons.

Earlier works used the factorized approximation to Eq. (8) above. This can be found by taking the t matrix in the integral, evaluating it at some energy, and pulling it out. The remaining integral then gives the density of the protons and neutrons. This approximation for the optical potential can be written in the simpler form [9,10]

$$\langle \mathbf{P}'_1|U(E)|\mathbf{P}_1\rangle = \rho_p(q)\langle\mathbf{P}'_1|t_{\pi p}(E)|\mathbf{P}_1\rangle + \rho_n(q)\langle\mathbf{P}'_1|t_{\pi n}(E)|\mathbf{P}_1\rangle, \quad (9)$$

where the subscripts p and n refer to the protons and neutrons. ρ is the density of the protons and neutrons, and q is introduced remind us that these densities are in momentum space.

We use a modified version of the computer code ROMPIN [7] to make our calculations. The results of 180 MeV π^+ scattering from ^{40}Ca are shown in Fig. 1. In the figure the solid curve is the result for RSE while the dash-dotted curve is the result for the KGE. The differences are substantial when compared to the results of Johnson and Ernst [3] at resonance. These differences are larger variations in the depths of the minimum and a change in the location of the minimum. Because the two-body amplitude is varying rapidly in this energy region, a shift in the energy at which the π-Nt matrix is evaluated can lead to substantial changes in the differential cross sections. We investigate this difference between the two approaches by adjusting the energy of the reaction and looking for the largest first minimum in the differential cross section. In this way we can determine the energy at which the two-body t matrix is evaluated at the P_{33} resonance. This is possible because we are scattering in the resonance region and the P_{33} resonance dominates the scattering [9]. For the KGE the minimum is found at 119 MeV while for the RSE it is at 135 MeV. This gives a difference of 16 MeV. We can conclude that in the calculations of the KGE and the RSE at 180 MeV, the two-body t matrices were evaluated at energies that differed by approximately 16 MeV. Such an energy shift can account for the observed differences in the calculated cross section.

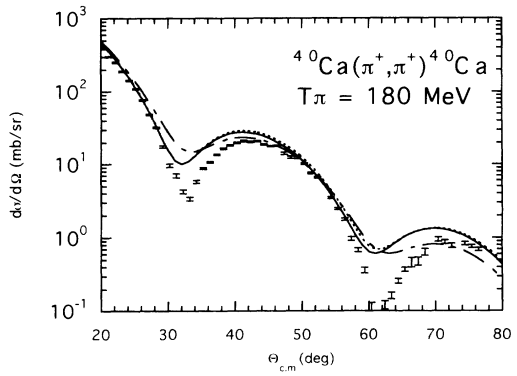

FIG. 1. The differential cross section for the ^{40}Ca(π^+,π^+)^{40}Ca reaction at 180 MeV. The solid curve is the RSE calculation, the dash-dotted curve is the KGE calculation, and the dotted curve is the KGE with the reduced range of the interaction. The data are from Ref. [16].

We can also adjust the range in the two-body form factor. This can have a large affect on the differential cross sections [12]. By adjusting the range from the modeled value of 978 MeV [13,6] in the P_{33} channel, to 350 MeV for the KGE, we get the dashed curve in Fig. 1. The agreement is almost exact at the first minimum and gradually becomes worse as the angles increase. Thus, the KGE calculation has the affect of lengthening the effective range of the π-N interaction (shorter range in configuration space) when compared to the RSE. This increase in the effective range of the π-N interaction would make little difference in the differential cross sections at this energy when the factorized approximation is used [14]. It was not possible to adjust the range in the RSE to reproduce the KGE results. The range was increased until the point source limit was reached. Even in this limit, the original KGE results could not be reproduced by the RSE.

To further investigate the source of the difference between the two approaches, we ran the KGE with the separable potential off-shell behavior and the RSE with the Chew-Low behavior. In Figs. 2 and 3 we see the results for these calculations compared to the earlier results. No data were plotted for clarity of the curves. In Fig. 2 we see in the first minimum that the large difference between the KGE calculation and the RSE calculation was due, primarily, to the off-shell behavior. The four curves

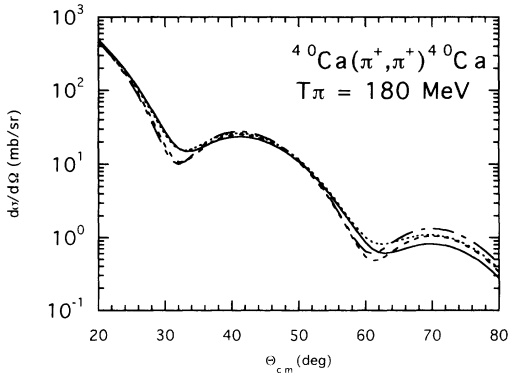

FIG. 2. The differential cross section for the ^{40}Ca(π^+,π^+)^{40}Ca reaction at 180 MeV. The solid curve is the standard KGE calculation (Chew-Low off-shell), the dotted curve is for the RSE with the Chew-Low off-shell behavior, the dash-dotted curve is the standard RSE calculation (separable off-shell), and the short dashed curve is the KGE with the separable off-shell behavior. No data are shown for clarity of the curves.

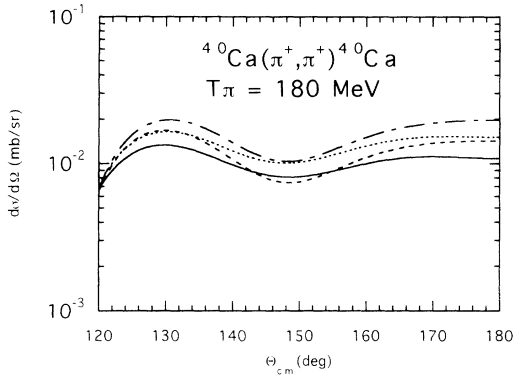

FIG. 3. Same as for Fig. 2 except the scattering angles are from 120° to 180°.

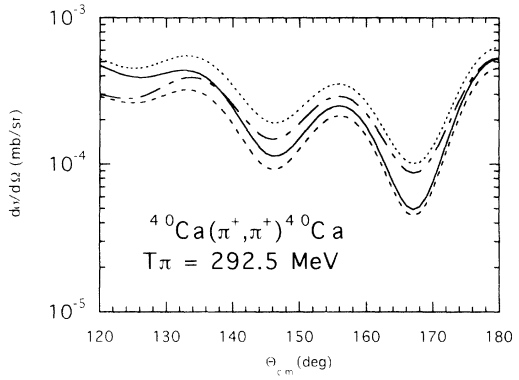

FIG. 5. Same as for Fig. 4 except the scattering angles are from 120° to 180°.

plotted break into two pairs, one pair for the Chew-Low option and the other for the separable potential option. While this can be clearly seen in the first minimum, the curves do not decompose in the second minimum. Thus, at small angles, the off-shell behavior is the most important factor in determining the differences observed in the differential cross sections. In Fig. 3, the situation is quite different. Looking at the last minimum in the differential cross section, we see that the four curves have split into two pairs by the equation that was solved, that is, by the propagator used. The two KGE calculations are closer together and the two RSE calculations are closer together. Thus, at large angles, the equation solved would seem to have more of an influence on the differential cross sections than the off-shell behavior. Since the KGE used contains crossing, this symmetry has a large enough influence that it should not be ignored. Even at these large angles, the influence of the off-shell option can be seen in the overall shape of the differential cross sections.

As we increase the energy, above resonance, we would expect the two calculations to agree. In Fig. 4 we see that at 292.5 MeV the two calculations still do not agree although the difference is less than that at 180 MeV. The interplay of the propagator and the off-shell behavior is still very complex at this energy. This can be seen in Fig. 5 where at the minimum near 125° the four curves group into pairs by which propagator is used while at the minimum near 169° the four curves split into pairs by which off-shell behavior is used. In Fig. 5 we can also see that there is still a rather large difference between the two calculations that is not so obvious on a semilogarithmic plot at forward angles. This difference persists to higher energies. At 500 MeV, we can see a substantial difference between the two calculations in Fig. 6. The field theoretic calculation is almost a factor of 2 larger at all angles [15]. Once again we performed calculations using the separable potential off-shell behavior with the KGE and using the Chew-Low off-shell behavior with the RSE. It is found that at this high energy, the difference between the two curves is dominated by the off-shell behavior with only a small difference from the propagator used. Very similar results were found for 400 MeV as well. For this reason, we may expect this difference between the two calculations to continue at even higher energies.

We conclude that the field theoretic off-shell behavior and crossing symmetry found in the KGE are important in the resonance region when the Fermi integral is performed. This is contrary to earlier results that relied on the factorized approximation to the Fermi integral and found close agreement between the two equations near resonance. The use of the RSE, which does not include this symmetry and has a separable potential off-shell behavior, is inadequate in the resonance region. At small angles, the off-shell behavior dominates the differences

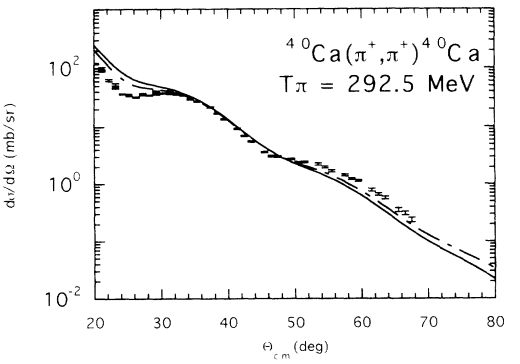

FIG. 4. The differential cross section for the $^{40}Ca(\pi^+,\pi^+)^{40}Ca$ reaction at 292.5 MeV. The solid curve is the RSE calculation; the dash-dotted curve is the KGE calculation. The data are from Ref. [16].

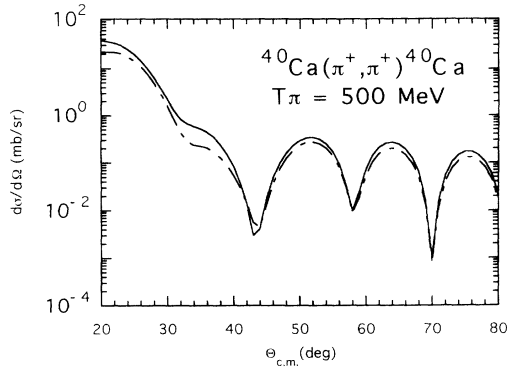

FIG. 6. Same as for Fig. 4 except for 500 MeV.

between the two approaches. This would be due to calculating the Fermi integral in determining the optical potential which magnifies the differences in the off-shell options. For consistency, one should use the Chew-Low options with the KGE and the separable potential with the RSE. At small angles, this difference can be understood as an effect energy shift of 16 MeV of the evaluation of the two-body t matrix. It can also be understood as an effective increase in the range of the interaction in the P_{33} channel, in the KGE, from 350 to 978 MeV. The RSE could not be adjusted in a simple way to account for its difference with the KGE.

At high energies, the difference between the two calculations was primarily due to the two different off-shell behaviors used. At energies as high as 500 MeV the difference was still almost a factor of 2 at all angles [15]. It would appear from these calculations that the two different approaches will not agree at high energies, when the Fermi integral is performed. It would be incorrect to infer that one could use the field theoretic off-shell behavior with the RSE in order to improve its accuracy since such a calculation would be inconsistent. One should be aware of this difference when performing high energy calculations. The author feels that the difference is large enough that only the Klein-Gordon equations should be used even at high energies when the Fermi integral is calculated to find the optical potential.

This work was supported, in part, by Associated Western Universities. The author would like to thank David J. Ernst and Mikkel B. Johnson for some enlightening conversations and LAMPF at Los Alamos National Laboratory for its hospitality during part of this work.

[1] L. S. Kisslinger, Phys. Rev. **98**, 761 (1955); M. Ericson and T. E. O. Ericson, Nucl. Phys. **B11**, 521 (1969); G. E. Brown and W. Weise, Phys. Rep. **22**, 909 (1975); J. Nieves, E. Oset, and C. Garcia-Recio, Nucl. Phys. **A554**, 554 (1993).

[2] R. H. Landau, S. C. Phatak, and F. Tabakin, Ann. Phys. (N.Y.) **78**, 299 (1973); E. R. Siciliano and G. E. Walker, Phys. Rev. C **13**, 257 (1976); R. H. Landau and A. W. Thomas, Nucl. Phys. **A302**, 461 (1978); M. Arima, K. Masutani, and R. Seki, Phys. Rev. C **44**, 415 (1991).

[3] M. B. Johnson and D. J. Ernst, Phys. Rev. C **20**, 1064 (1979).

[4] D. J. Ernst and M. B. Johnson, Phys. Rev. C **24**, 2210 (1981).

[5] M. B. Johnson and D. J. Ernst, Phys. Rev. C **27**, 709 (1983).

[6] D. J. Ernst and M. B. Johnson, Phys. Rev. C **22**, 651 (1980).

[7] D. R. Giebink and D. J. Ernst, Comput. Phys. Commun. **48**, 407 (1988).

[8] M. B. Johnson and D. J. Ernst, Phys. Rev. C **27**, 709 (1983); D. J. Ernst, in Proceedings of the Spring School on Medium- and High-Energy Nuclear Physics, Taipei, Taiwan, 1988 (unpublished).

[9] A. W. Thomas and R. H. Landau, Phys. Rep. **58**, 121 (1980).

[10] K. A. Eisenstein and F. Tabakin, Comput. Phys. Commun. **12**, 237 (1976).

[11] The P_{11} channel is treated differently because of the nucleon pole [7]. This different treatment is not important here since the P_{33} channel dominates at resonance while at higher energies other π-N partial waves contribute to the cross section.

[12] R. J. McLeod and Xiaodan Ren, Phys. Rev. C (submitted); Xiaodan Ren, Idaho State University M.S. thesis, 1992 (unpublished).

[13] D. J. Ernst and M. B. Johnson, Phys. Rev. C **17**, 247 (1978).

[14] R. J. McLeod and E. R. Siciliano, Bull. Am. Phys. Soc. **26**, 566 (1981).

[15] This difference is for all angles, out to 180°, except for the forward angles where the Coulomb interaction dominates.

[16] K. G. Boyer, W. J. Braithwaite, W. B. Cottingame, S. J. Greene, L. E. Smith, C. F. Moore, C. L. Morris, H. A. Thiessen, G. B. Blampied, G. R. Burleson, J. F. Davis, J. S. McCarthy, R. C. Minehart, and C. A. Goulding, Phys. Rev. C **29**, 182 (1984).